Electrochemical and Solid-State Letters, **12** (1) B1-B4 (2009)
1099-0062/2008/12(1)/B1/4/$23.00 © The Electrochemical Society

Nanostructured Pt–$Sn_{1-x}In_xP_2O_7$ Cathodes for High-Temperature Proton Exchange Membrane Fuel Cells

Pilwon Heo,* Toshihiko Harada, and Takashi Hibino,z**

Graduate School of Environmental Studies, Nagoya University, Nagoya 464-8601, Japan

Nanosized proton-conducting $Sn_{0.95}In_{0.05}P_2O_7$ ionomers were grown on carbon supports by the coprecipitation of tin and indium chlorides with excess ammonia water and subsequent solid-state reaction with phosphoric acid. The resulting homogeneous networks of $Sn_{0.95}In_{0.05}P_2O_7$ ionomers enhanced the activity of a Pt catalyst for the oxygen reduction reaction in the temperature range of 150–250°C. In addition, the Pt catalyst showed high corrosion resistance in the cathode environment while maintaining high performance levels. A comparison of the cathode performance between $Sn_{0.95}In_{0.05}P_2O_7$ and H_3PO_4 ionomers further demonstrated that the $Sn_{0.95}In_{0.05}P_2O_7$ nanoparticles are promising candidates for cathode ionomer materials at high temperatures.
 [DOI: 10.1149/1.3006328]

Manuscript submitted July 31, 2008; revised manuscript received September 29, 2008. Published October 27, 2008.

Proton exchange membrane fuel cells (PEMFCs) are considered to be the most suitable for vehicular and residential applications, and development of this technology has been aggressively driven toward commercialization.[1] A recent trend in developing PEMFCs is to increase the operating temperature up to 120°C or higher and to decrease the relative humidity needed up to as low a value as possible, which offers many advantages over conventional PEMFCs operating at ~80°C.[2,3] Operating a fuel cell at elevated temperatures provides high CO tolerance of the anode catalyst, eliminating the need for a CO removal unit (water-gas-shift and CO preferential oxidation reactors). Also, electrode reaction kinetics are enhanced by increasing the temperature, allowing for low Pt loadings. Other advantages include simplified water management, good drainage at the cathode, and effective heat dissipation.

A number of high-temperature PEMFCs based on different types of proton conductors have been reported over the past decade.[4-8] We previously found that a fuel cell using In^{3+}-doped SnP_2O_7 ($Sn_{1-x}In_xP_2O_7$) as an electrolyte membrane showed high stability between 100 and 300°C in unhumidified atmospheres.[9] This fuel cell allowed operation even at 10% CO concentration[10] and enabled the use of alternative anodes to Pt.[11] However, contrary to expectations, the catalytic activity of the Pt/C cathode for the oxygen reduction reaction (ORR) was not sufficiently high to yield good cell performance. One of the main reasons for the poor ORR activity is thought to be the lack of proton conduction in the catalyst layer. The ORR occurs at the three-phase boundary (TPB) (gas-phase/electrode/electrolyte) where all electrons, protons, and gases are available. It is difficult for high-temperature PEMFCs to use organic proton conductors, such as Nafion, as ionomers since they dehydrate at elevated temperatures and at low relative humidities, losing their proton conducting properties. Although liquid H_3PO_4 is sometimes used as an ionomer for the cathode, it has a serious challenge in that the Pt catalyst is subjected to corrosion.[12,13] Another challenge for the H_3PO_4 ionomer is the poisoning of the Pt catalyst by strong adsorption of phosphate anions.[14] Thus, the development of ionomers is critical to ensure successful working of high-temperature PEMFCs.

In this study, we propose an approach for designing a three-dimensional network of Pt, ionomer, and carbon particles in the catalyst layer. Our approach is based on the following: (*i*) $Sn_{1-x}In_xP_2O_7$ exhibits high proton conductivities (~0.1 S cm^{-1}) between 100 and 300°C in dry and wet conditions, (*ii*) both SnO_2 and In_2O_3 easily react with H_3PO_4 to form $Sn_{1-x}In_xP_2O_7$ with cluster sizes of several tens of nanometers, and (*iii*) $Sn_{1-x}In_xP_2O_7$ is an inorganic compound with high chemical and electrochemical stability. We demonstrate that Pt–$Sn_{1-x}In_xP_2O_7$ nanoparticles provide many reaction sites for the ORR and high corrosion resistance of Pt in the cathode environment, so that the activity and stability of the cathode are significantly improved at high temperatures.

Experimental

Preparation of the nanostructured cathodes.— First, $Sn_{1-x}In_xP_2O_7$/C catalyst powders were prepared by coprecipitation and subsequent solid-state reaction. Appropriate quantities of $SnCl_4 \cdot 5H_2O$ and $InCl_3 \cdot 4H_2O$ were suspended with carbon powders (Black Pearls) in distilled water while stirring at room temperature. A 10 wt % NH_3 aqueous solution was added dropwise to the suspension until a final pH value of ~8 was obtained. The precipitate was filtered and then washed with distilled water. After drying at 100°C, the powders were heated in a flowing Ar atmosphere at 600°C for 2 h. The product was mixed with 85% H_3PO_4 in a mortar and pestle, and then heated in a similar manner to the above procedure. Second, Pt–$Sn_{1-x}In_xP_2O_7$/C catalyst powders were prepared by chemical reduction of Pt precursors using $NaBH_4$ as a reducing agent. The $Sn_{1-x}In_xP_2O_7$/C powders were suspended in distilled water. Two aqueous solutions of 0.8 wt % $H_2PtCl_6 \cdot 6H_2O$ and 1.1 wt % $NaBH_4$ were simultaneously added into the suspension while stirring at 70°C. The mixture solution was stirred for 1 h, filtered, and finally washed with distilled water. After drying at 100°C, the powders were heated in a H_2/Ar (10 vol % H_2) mixture feed at 200°C for 1 h. Unless otherwise stated, the $Sn_{1-x}In_xP_2O_7$ and Pt weight percentages of the catalyst powders obtained were 69 and 9%, respectively. Also, the In content in $Sn_{1-x}In_xP_2O_7$ was 0.05. Finally, the Pt–$Sn_{1-x}In_xP_2O_7$/C powders were mixed with polytetrafluoroethylene (PTFE) binder in a glycerin solvent using the mortar and pestle. The mixture was coated on a gas diffusion layer (Toray TGPH-090), followed by heating at 350°C for 1 h. Pt/C, Pt/C impregnated with H_3PO_4 (hereafter, "Pt/C + H_3PO_4"), and a physical mixture of Pt/C and $Sn_{0.95}In_{0.05}P_2O_7$ powders with the same content as Pt–$Sn_{0.95}In_{0.05}P_2O_7$/C (hereafter, "Pt/C + $Sn_{0.95}In_{0.05}P_2O_7$") were used for comparison. The compositions of the four cathodes are as follows; 44 wt % $Sn_{1-x}In_xP_2O_7$, 6 wt % Pt, 14 wt % C, and 36 wt % PTFE for the Pt–$Sn_{1-x}In_xP_2O_7$/C and Pt/C + $Sn_{0.95}In_{0.05}P_2O_7$ cathodes; 13 wt % Pt, 30 wt % C, and 57 wt % PTFE for the Pt/C and Pt/C + H_3PO_4 cathodes. The loading of Pt was controlled at 0.6 mg cm^{-2} for all the cathodes.

Synthesis of the electrolyte membrane.— An $Sn_{0.9}In_{0.1}P_2O_7$ electrolyte membrane was synthesized in the same manner as previously reported.[9-11] The corresponding oxides (SnO_2 and In_2O_3) were mixed with 85% H_3PO_4 and ion-exchanged water and then held while stirring at 300°C until a high viscosity paste was formed. The paste was calcined in an alumina pot at 650°C for 2.5 h and then ground in a mortar with a pestle. PTFE powders were added to the $Sn_{0.9}In_{0.1}P_2O_7$ powders with 10 wt % PTFE and 90 wt % $Sn_{0.9}In_{0.1}P_2O_7$, then kneaded using the mortar and pestle, and finally cold rolled to a thickness of 0.1 mm.

* Electrochemical Society Student Member.
** Electrochemical Society Active Member.
z E-mail: hibino@urban.env.nagoya-u.ac.jp

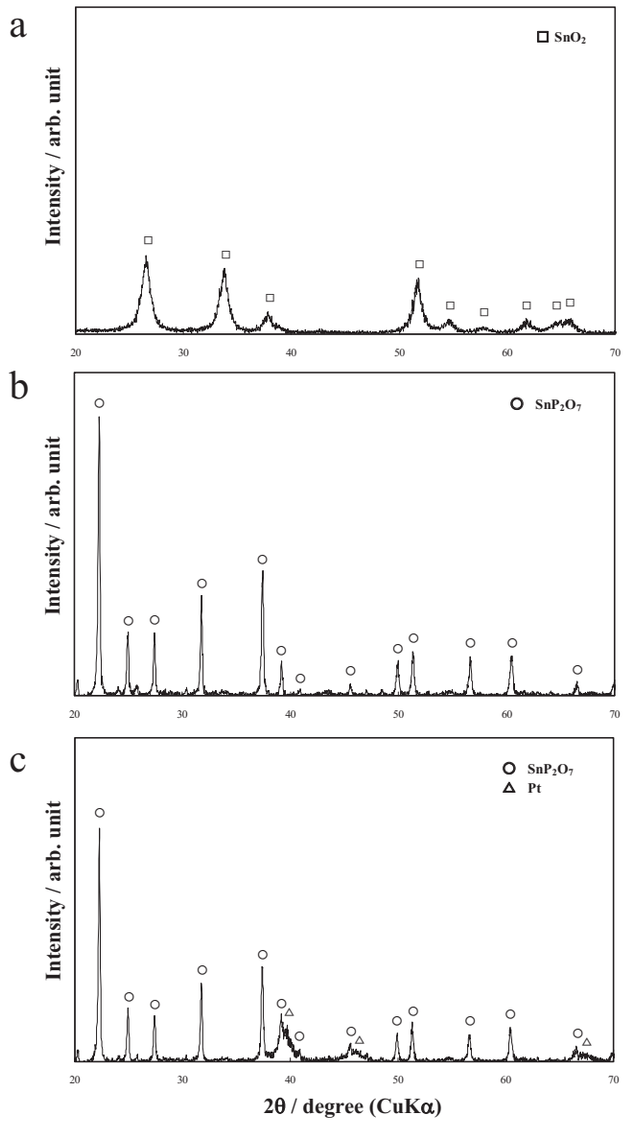

Figure 1. XRD profiles of (a) sample powders prepared by coprecipitation of $SnCl_4 \cdot 5H_2O$ and $InCl_3 \cdot 4H_2O$ with NH_3 aqueous solution and subsequent heat-treatment at 600°C, (b) sample powders prepared by a solid-state reaction with H_3PO_4 at 600°C, and (c) sample powders prepared by chemical reduction of $H_2PtCl_6 \cdot 6H_2O$ using $NaBH_4$ as a reducing agent.

Characterization of the cathodes.— The microstructures of the catalyst powders were analyzed using X-ray diffraction (XRD), scanning electron microscopy (SEM), and transmission electron microscopy (TEM). The overpotentials and impedance spectra of the cathodes were analyzed by the current interruption and complex impedance methods, respectively. A Pt/C anode (10 wt % Pt/C, 0.6 mg Pt cm^{-2}) was purchased from E-TEK, Inc. The anode and cathode (area: 0.5 cm^2) were attached on opposite sides of the electrolyte. A Pt reference electrode was attached on the surface of the side of the electrolyte. Two gas chambers were set up by placing the cell assembly between two alumina tubes. The anode and cathode chambers were supplied with unhumidified hydrogen and air, respectively, at a flow rate of 30 mL min^{-1} in the temperature range from 150 to 300°C.

Results and Discussion

$Pt–Sn_{0.95}In_{0.05}P_2O_7/C$ powders were prepared step by step and characterized at each step using XRD. In the first step, $Sn(OH)_4$ and $In(OH)_3$ were precipitated on the carbon support, followed by heat-treatment at 600°C in Ar. Figure 1a shows the XRD profile of the obtained powders. All the diffraction peaks observed were assigned to the SnO_2 tetragonal structure, suggesting that 5 mol % In^{3+} cations are substituted for a part of Sn^{4+} cations in SnO_2. In the second step, the powders were treated with H_3PO_4 and then heated at 600°C in Ar. As shown in Fig. 1b, the diffraction pattern of the powders was identical to the SnP_2O_7 cubic structure[15] and no other metal oxide peaks were observed, indicating that $Sn_{0.95}In_{0.05}O_2$ reacted with H_3PO_4 to form $Sn_{0.95}In_{0.05}P_2O_7$ on the carbon support. The mean particle size of $Sn_{0.95}In_{0.05}P_2O_7$, estimated using the Scherrer formula, was found to be 62 nm, which is considerably smaller than the ~500 nm size estimated for $Sn_{0.95}In_{0.05}P_2O_7$ prepared by a solid-state reaction of SnO_2, In_2O_3, and H_3PO_4 without any added carbon. It is likely that the metal hydroxides formed in the first step are highly dispersed on the carbon support, resulting in a small particle size of $Sn_{0.95}In_{0.05}P_2O_7$. At the final step, Pt particles were impregnated in the $Sn_{0.95}In_{0.05}P_2O_7/C$ powders. In the XRD profile shown in Fig. 1c, very small diffraction peaks assigned to Pt were observed along with those assigned to SnP_2O_7. Although the particle size of Pt could not be estimated from the XRD data due to the low resolution, TEM showed that the particle sizes of Pt were in the range of 3–7 nm, as described later. Therefore, it is evident that both $Sn_{0.95}In_{0.05}P_2O_7$ and Pt nanoparticles were grown on the carbon support. Note that it was very difficult to prepare $Sn_{0.95}In_{0.05}P_2O_7$ particles in the case of previously prepared Pt/C powders, because an alloy of Pt and Sn was formed in the subsequent heat-treatment.

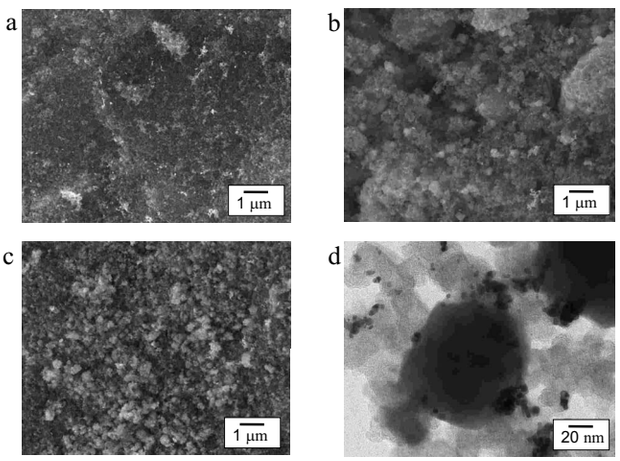

Figure 2. SEM micrographs of (a) H_3PO_4-impregnated Pt/C (Pt/C + H_3PO_4), (b) $Sn_{0.95}In_{0.05}P_2O_7$-mixed Pt/C (Pt/C + $Sn_{0.95}In_{0.05}P_2O_7$), and (c) $Sn_{0.95}In_{0.05}P_2O_7$-grown Pt/C ($Pt–Sn_{0.95}In_{0.05}P_2O_7/C$). (d) TEM micrograph of $Pt–Sn_{0.95}In_{0.05}P_2O_7/C$.

The microstructure of the $Pt–Sn_{0.95}In_{0.05}P_2O_7/C$ powders is shown in Fig. 2, including the data for the Pt/C + H_3PO_4 and Pt/C + $Sn_{0.95}In_{0.05}P_2O_7$ cathodes. By comparing the microstructures among the three catalyst powders, it was seen that there were several micron-sized agglomerates of $Sn_{0.95}In_{0.05}P_2O_7$ primary particles in the Pt/C + $Sn_{0.95}In_{0.05}P_2O_7$ matrix (Fig. 2b) and several hundreds of nanometer sized agglomerates of $Sn_{0.95}In_{0.05}P_2O_7$ primary particles in the $Pt–Sn_{0.95}In_{0.05}P_2O_7/C$ matrix (Fig. 2c). Moreover, the agglomerates of $Sn_{0.95}In_{0.05}P_2O_7$ primary particles were more homogeneously and closely connected with each other in the $Pt–Sn_{0.95}In_{0.05}P_2O_7/C$ matrix, compared to those in the Pt/C + $Sn_{0.95}In_{0.05}P_2O_7$ matrix. A TEM image of the $Pt–Sn_{0.95}In_{0.05}P_2O_7/C$ is shown in Fig. 2d. It is observed that the primary particle sizes of $Sn_{0.95}In_{0.05}P_2O_7$ and Pt were about 80 and 5 nm, respectively, wherein the Pt particles were deposited not only on the carbon but also on the $Sn_{0.95}In_{0.05}P_2O_7$ primary particles. The

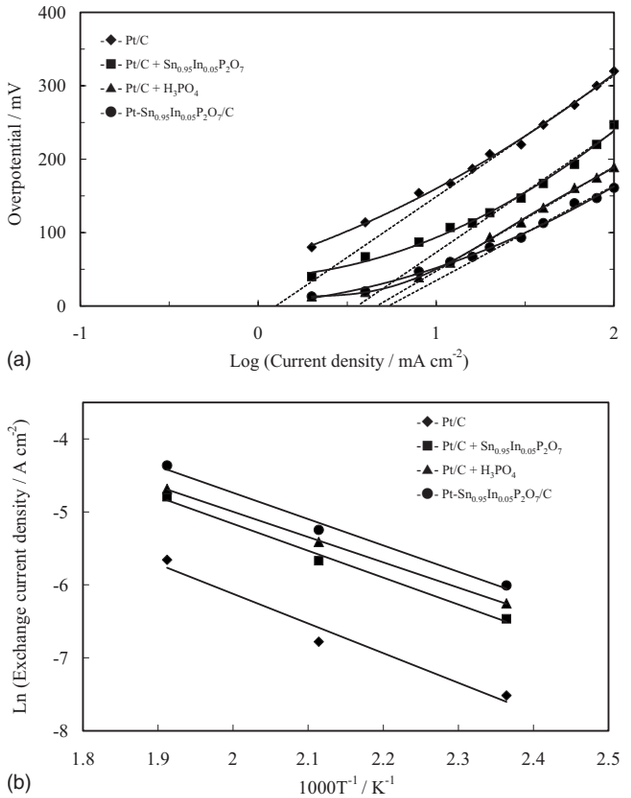

Figure 3. (a) Tafel plots of untreated Pt/C, Pt/C + H_3PO_4, Pt/C + $Sn_{0.95}In_{0.05}P_2O_7$, and Pt–$Sn_{0.95}In_{0.05}P_2O_7$/C cathodes for ORR at 200°C. (b) Arrhenius plots of exchange current density for untreated Pt/C, Pt/C + H_3PO_4, Pt/C + $Sn_{0.95}In_{0.05}P_2O_7$, and Pt–$Sn_{0.95}In_{0.05}P_2O_7$/C cathodes.

SEM and TEM observations suggest that the area of the TPB is much larger for the Pt–$Sn_{0.95}In_{0.05}P_2O_7$/C than for the Pt/C + $Sn_{0.95}In_{0.05}P_2O_7$.

The above suggestion was examined by measuring the cathodic properties of the Pt–$Sn_{0.95}In_{0.05}P_2O_7$/C. Figure 3a shows the Tafel plots of the overpotential for the different cathodes, including Pt–$Sn_{0.95}In_{0.05}P_2O_7$/C, Pt/C, Pt/C + H_3PO_4, and Pt/C + $Sn_{0.95}In_{0.05}P_2O_7$, at 200°C. The overpotential decreased on the order of Pt/C > Pt/C + $Sn_{0.95}In_{0.05}P_2O_7$ > Pt/C + H_3PO_4 > Pt–$Sn_{0.95}In_{0.05}P_2O_7$/C. This same order was also observed at 150 and 250°C. The Tafel slopes estimated for the four cathodes are shown in Table I. The Pt–$Sn_{0.95}In_{0.05}P_2O_7$/C cathode showed the smallest Tafel slope among the four cathodes. This means that the charge transfer in the ORR was considerably improved by the dispersion of $Sn_{0.95}In_{0.05}P_2O_7$ on the carbon surface, which is due to an enhanced turnover rate of Pt or an increased number of the reaction

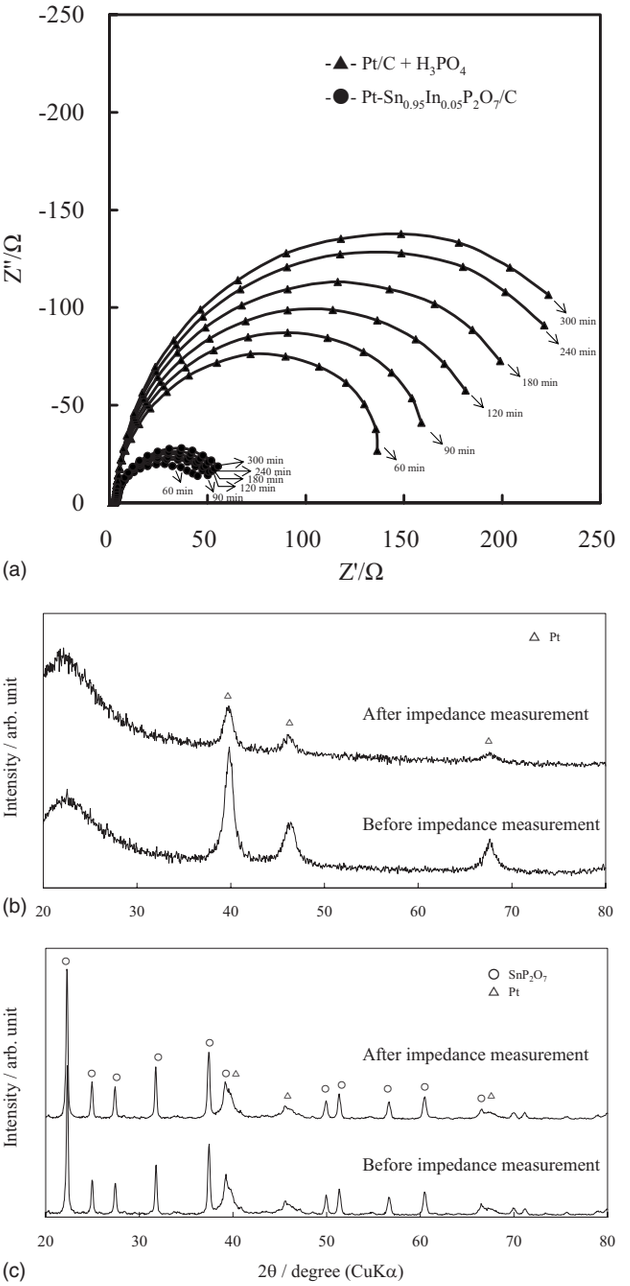

Figure 4. (a) Changes in the impedance spectra of Pt/C + H_3PO_4 and Pt–$Sn_{0.95}In_{0.05}P_2O_7$ cathodes over time at 200°C under open-circuit conditions. XRD profiles of (b) Pt/C + H_3PO_4 and (c) Pt–$Sn_{0.95}In_{0.05}P_2O_7$ before and after impedance measurements.

Table I. Kinetic values for ORR over various cathodes.

Sample	Tafel slope at 200°C (mV at decade^{-1})	Exchange current density (i_0) at 200°C (mA cm^{-2})	Apparent activation energy (E_a) (kJ mol^{-1})	Frequency factor (A)[a] (mA cm^{-2})
Pt/C	161.6	1.14	33.8	1.15
Pt/C + $Sn_{0.95}In_{0.05}P_2O_7$	161.8	3.45	30.6	3.48
Pt/C + H_3PO_4	140.6	4.47	28.9	4.50
Pt–$Sn_{0.95}In_{0.05}P_2O_7$/C	126.9	5.27	30.0	5.31

[a] $\ln i_0 = \ln A - (E_a/RT)$.

site. In order to clarify which factor is more important, we determined the exchange current densities for the four cathodes by using[16]

$$\eta = \frac{2.303RT}{n\alpha F} \log \frac{i}{i_0} \quad [1]$$

where η is the overpotential, R is the gas constant, F is Faraday's constant, n is the number of exchanged electrons, α is the transfer coefficient, and i and i_0 are the current density and exchange current density, respectively. The Arrhenius plots of the i_0 value for the four cathodes are shown in Fig. 3b. The apparent activation energies, E_a, for the four cathodes obtained from their slopes were close to one another (Table I), suggesting that the same reaction mechanism for the ORR was operating at the four cathodes. We consider that the differences in the i_0 values among the four cathodes arises from the differences in the frequency factor, A (Table I). It is reasonable to consider that the A value reflects the number of reaction sites at the cathode, which are responsible for the microstructure of the TPB in the cathode. On the basis of the above consideration, the high activity of the Pt–$Sn_{0.95}In_{0.05}P_2O_7$/C cathode for the ORR can be attributed to the large area of the TPB provided by the $Sn_{0.95}In_{0.05}P_2O_7$ nanoparticles.

The carbon-supported $Sn_{0.95}In_{0.05}P_2O_7$ nanoparticles could reduce the overpotential of the Pt/C cathode for the ORR. However, we still cannot explain why the Pt–$Sn_{0.95}In_{0.05}P_2O_7$/C cathode shows better performance than the Pt/C + H_3PO_4 cathode, since both cathodes have various sufficient proton pathways and reaction sites. One possible explanation is that the Pt/C + H_3PO_4 cathode deteriorates during the above polarization measurements. The impedance spectra of the two cathodes were therefore compared at open-circuit voltage (OCV). It can be seen from Fig. 4a that while the Pt/C + H_3PO_4 cathode showed considerably increased polarization resistance with time, the Pt–$Sn_{0.95}In_{0.05}P_2O_7$/C cathode showed relatively high stability of the polarization resistance. These results can be better understood from the XRD profiles of the two cathodes before and after the impedance measurements shown in Fig. 4b and c. After the measurements, the diffraction peak intensities of Pt were significantly reduced for the Pt/C + H_3PO_4 cathode; however, changes in the diffraction peaks were very small for the Pt–$Sn_{0.95}In_{0.05}P_2O_7$/C cathode. Therefore, the degradation of the Pt/C + H_3PO_4 cathode is considered to be due to the dissolution of Pt in the ionomer at high cathode potentials[17,18] or the agglomeration of Pt particles caused by carbon corrosion.[13,19] This suggests that the high stability of the Pt–$Sn_{0.95}In_{0.05}P_2O_7$/C cathode can be attributed to the low solubility of Pt and carbon in the $Sn_{0.95}In_{0.05}P_2O_7$ nanoparticles.

Conclusions

We successfully prepared ~80 nm $Sn_{0.95}In_{0.05}P_2O_7$ particles and ~5 nm Pt particles on the surface of the carbon support. This preparation method suppressed the growth of $Sn_{0.95}In_{0.05}P_2O_7$ particles into micron-sized agglomerates and formed more homogeneously connected networks on the cathode. For various Pt/C cathodes, polarization measurements revealed that the $Sn_{0.95}In_{0.05}P_2O_7$-grown Pt/C cathode exhibited ORR activity comparable to or higher than that observed for a H_3PO_4-impregnated Pt/C cathode, due to the significant increase in the number of reaction sites for the ORR. Another beneficial effect of this preparation method was the higher stability of the cathode at OCV, compared to that of the H_3PO_4-impregnated Pt/C cathode. This stability was responsible for the low solubility of Pt and carbon in the $Sn_{0.95}In_{0.05}P_2O_7$ particles.

Nagoya University assisted in meeting the publication costs of this article.

References

1. B. C. H. Steele and A. Heinzel, *Nature (London)*, **414**, 345 (2001).
2. Q. Li, R. He, J. O. Jensen, and N. J. Bjerrum, *Chem. Mater.*, **15**, 4896 (2003).
3. J. Zhang, Z. Xie, J. Zhang, Y. Tang, C. Song, T. Navessin, Z. Shi, D. Song, H. Wang, D. P. Wilkinson, et al., *J. Power Sources*, **160**, 872 (2006).
4. S. M. J. Zaidi, S. D. Mikhailenko, G. P. Robertson, M. D. Guiver, and S. Kaliaguine, *J. Membr. Sci.*, **173**, 17 (2000).
5. O. Savadogo and B. Xing, *J. New Mater. Electrochem. Syst.*, **3**, 343 (2000).
6. P. Genova-Dimitrova, B. Baradie, D. Foscallo, C. Poinsingnon, and J. Y. Sanchez, *J. Membr. Sci.*, **185**, 59 (2001).
7. K. T. Adjemian, S. Srinivasan, J. Benziger, and A. B. Bocarsly, *J. Power Sources*, **109**, 356 (2002).
8. T. Matsui, T. Kukino, R. Kikuchi, and K. Eguchi, *Electrochem. Solid-State Lett.*, **8**, A256 (2005).
9. M. Nagao, A. Takeuchi, P. Heo, T. Hibino, M. Sano, and A. Tomita, *Electrochem. Solid-State Lett.*, **9**, A105 (2006).
10. P. Heo, H. Shibata, M. Nagao, T. Hibino, and M. Sano, *J. Electrochem. Soc.*, **153**, A897 (2006).
11. P. Heo, M. Nagao, M. Sano, and T. Hibino, *J. Electrochem. Soc.*, **154**, B53 (2007).
12. J. Lobato, P. Cañizares, M. A. Rodrigo, and J. Linares, *Electrochim. Acta*, **52**, 3910 (2007).
13. Z. Qi and S. Buelte, *J. Power Sources*, **161**, 1126 (2006).
14. D. A. Landsman and F. J. Luczak, *Handbook of Fuel Cells—Fundamentals, Technology and Applications*, Vol. 4, p. 811, John Wiley & Sons, Hoboken, NJ (2003).
15. P. K. Gover, N. D. Withers, S. Allen, R. L. Withers, and S. O. Evans, *J. Solid State Chem.*, **166**, 42 (2002).
16. O. A. Petrii, R. R. Nazmutdinov, M. D. Bronshtein, and G. A. Tsirlina, *Electrochim. Acta*, **52**, 3493 (2007).
17. P. J. Ferreira, G. J. La O', Y. Shao-Horn, D. Morgan, R. Makharia, S. Kocha, and H. A. Gasteiger, *J. Electrochem. Soc.*, **152**, A2256 (2005).
18. R. M. Darling and J. P. Meyers, *J. Electrochem. Soc.*, **152**, A242 (2005).
19. A. Honji, T. Mori, K. Tamura, and Y. Hishinuma, *J. Electrochem. Soc.*, **135**, 355 (1988).